Calibration of a multiple microchannel plate detectors system by α-induced secondary electrons

J. Villette, M. Barat, and P. Roncin

Laboratoire des Collisions Atomiques et Moléculaires, CNRS UMR 8625, Université Paris Sud, F-91405 Orsay, Cedex, France

α particles emitted from an [241]Am radioactive source at energies of 5.4 MeV generate bursts of about ten electrons when passing through an aluminized Mylar foil. Besides the typical surface barrier electrons, the energy spectra of the secondary electrons clearly reveal two additional peaks. One at 66 eV is ascribed to aluminum *LVV* Auger electrons and another at 10.5 eV is attributed to the decay of aluminum volume plasmons. The well-resolved angular and energy distributions of these secondary electrons are used to calibrate the relative detection efficiencies of a large set of individual detectors of a complex multicoincidence system. © *2000 American Institute of Physics.* [S0034-6748(00)05206-0]

I. INTRODUCTION

Experimental investigation of ion surface interaction leads to the development of specific detection setups able to analyze the reflected projectiles and various secondary particles in coincidence.[1,2] Secondary particles, such as electrons and sputtered and desorbed ions, are emitted in the whole half space above the target surface plane. In order to optimize their collection, a large acceptance 2π multidetector was developed.[1] It is composed of a large set of microchannel plate (MCP) based detectors located on a half sphere above the target surface allowing, in principle, direct evaluation of a coarse angular distribution. In practice, the detection efficiency of MCP detectors is very sensitive to numerous parameters such as, bias voltage, interplate acceleration, etc.[3] Accurate calibration of the detection efficiencies of all the MCP detectors is mandatory to derive absolute yields and correct angular distribution from these multidetector experiments. We have developed an *in situ* calibration procedure built around a compact radioactive source emitting α particles, each of them generating a burst of secondary electrons when passing through a foil. Taking the detection of the alpha particles as a starting signal, the time-of-flight (TOF) spectra of the secondary electrons recorded simultaneously on all the 15 electron detectors shows well-resolved peaks. Comparison of these spectra recorded in coincidence allows determination of the relative efficiency. This calibration procedure can be easily repeated, for instance, after each baking of the vessel.

II. EXPERIMENT

The experimental setup has been described in detail elsewhere[1] and only a brief account is given here. This device, which is dedicated to grazing ion surface scattering experiments, is able to detect in coincidence the scattered projectile and the secondary particles. The former is detected by a two-dimensional position-sensitive detector while the secondary particles (electrons, ions, etc.) ejected in the half space above the target are collected on a large acceptance

detector. For the present experiment, only the ''2π'' multidetector for secondary particles is used. It is composed of 16 individual detectors made of a stack of two microchannel plates of 30 mm active diameter and mounted on a hemisphere surrounding the target. Fifteen detectors are located 60 mm away from the target center and distributed on three rows (referred to as TOP, MID, and LOW) at, respectively, 30°, 55.5°, and 67.5° from the target normal (see Fig. 1). An additional detector (POLE in Fig. 1) is located at the top of the hemisphere, at 105 mm from the target. For each detector, the two MCPs are stacked in chevron and are simply separated by a 15 μm ring-shaped aluminum foil. Such assembly requires neither interplate acceleration voltage nor the use of matched-impedance MCPs. A simple resistive voltage divider[1] placed outside the UHV vessel allows fine tuning of both the overall bias voltage and the voltage ratio between the two MCPs. Before the experiment, all these voltage dividers are adjusted to produce a pulse-height distribution as narrow as possible. From one detector to the other, the gain may vary by nearly a factor of 2, whereas with the low threshold used in our setup the background noise varies from a few counts per second up to a worst-case value close to 50 counts per second. These comparatively large count rates remain negligible in multicoincidence experiments.

Each MCP detector covers an approximately 0.2 sr solid angle except the topmost detector which covers only 0.067 sr. This results in a total solid angle of 48.7% of the half space. Note, however, that the detector arrangement was chosen to optimize the upward geometrical coverage. Therefore, a cosine or a $\cos^2$ angular distribution of ejected particles leads, respectively, to 59% and 62% collection efficiency. Particles emitted from the surface drift freely to the 16 detection units of the 2π multidetector. Their energies are determined from their time of flight measured via a multichannel multihit time-to-digital converter (TDC).

During the calibration the target sample is replaced by a sealed radioactive source of [241]Am. The radioactive material
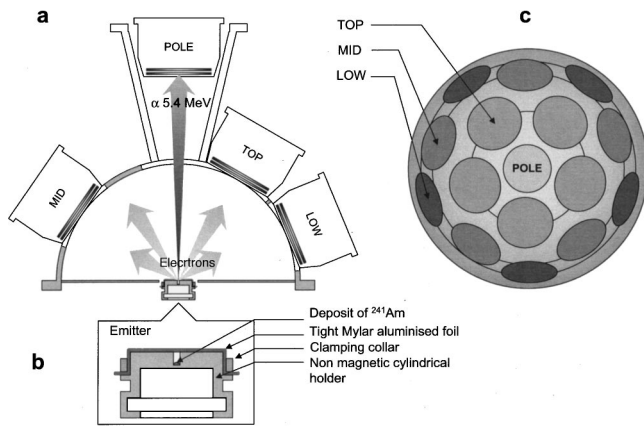
FIG. 1. (a) Cut view of the ''2π'' multidetector showing one detector from each of the three rows of five detectors (TOP, MID, and LOW rows) of five MCP based detectors. An additional polar detector (POLE) is located at the top of the hemisphere. (b) Enlarged view of the sealed radioactive source. The radioactive sample is embedded inside a cylindrical holder covered by an aluminized Mylar foil tight as a drumhead by a clamping collar. (c) Top view of the ''2π'' multidetector showing the azimuthal detector arrangement (active area).
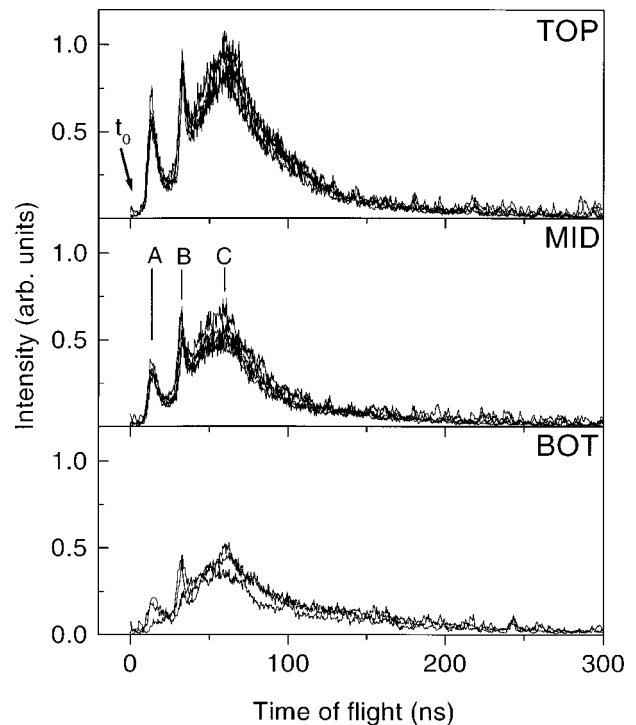

FIG. 2. Time-of-flight spectra of emitted electrons recorded on the top (TOP), middle (MID), and bottom (LOW) rows of the detectors. Each box shows the superimposed spectra of the five individual detectors (except for the bottom row in which two detectors were turned off). An arrow points to the origin time or impact time t_o, where the photon peak is observed.

is deposited by solvent evaporation at the bottom of a channel—1 mm in diameter and 2 mm in depth—drilled in a nonmagnetic alloy (AP4) cylinder. A 1.5-μm-thick Mylar foil, with a 1000 Å layer of aluminum on top of it, covers the cylinder. The ^{241}Am material with an activity of 2000 $\pm$ 1000 Becquerels (Bq) decays by emitting primarily 5443 and 5485 keV alpha particles and 59.50 keV gamma radiation.[4] Such source are commonly used as portable sources for gamma radiography and also as ionization sources in commercial smoke detectors. ^{241}Am was chosen because the recoil nuclei are not fast enough (92 keV) to pass through the foil, thus avoiding any vessel contamination with radionucleides. The relatively long half life (432.7 years) was found to be convenient for reproducible operation. Due to the geometrical configuration of the source, most of the alpha particles are absorbed within the cylinder wall and only a small fraction of the emitted particle flux strikes the Mylar foil near normal incidence. The aluminized film does not stop the α particles, which can then provide a start signal (Fig. 1) when reaching the pole detector biased at -500 V in order to reject all secondary electrons. The α particles lose only 120 keV/μm in Mylar and 155 keV/μm in aluminum, resulting in an average energy loss of 176 keV as calculated with the TRIM code.[5] The resulting energy spread leads to insignificant uncertainty in the trigger time. The secondary electrons drift freely toward the detectors in a field-free region defined by a hemispherical grid, and are finally postaccelerated before they hit the frontside of the channel-plate biased at $+500$ V. This ensures that the detection efficiency does not depend on the initial electron energy in the range considered here. Moreover, the MCP detection efficiency peaks around 200–500 eV.[6] In addition, this electric field, which attracts back the secondary electrons emitted from the ''blind'' interchannel web, increases significantly the detection efficiency.[7] The arrival times of the secondary electrons are simultaneously recorded with a 0.5 ns resolution on 15 channels of a multihit TDC (LeCroy 3377). We thus get the

energy spectra as well as the spatial distribution of the emitted electrons.

An activity of 1940 Bq for our ^{241}Am source can be estimated from the average 10 hits/s counting rate measured on the pole detector. Assuming an almost 100% counting efficiency, this disintegration rate (activity) is easily calculated as the measured count rate times the 4π solid angle and divided by the 0.067 sr solid angle seen by the pole detector. The data are acquired during, typically, 10 h in order to provide sufficient statistics.

III. ANGULAR DISTRIBUTION

Figure 2 shows TOF spectra measured on the three series of detectors. All spectra are nearly identical and composed of three peaks labeled A, B, and C. The latter corresponds to low-energy secondary electrons, whereas the two sharp peaks are most likely due to the decay of atomic or solid-state resonance and will be discussed in the next section.

Only α particles that strike the Mylar along the near-normal axis hit the topmost detector and then trigger the acquisition, thus providing a cylindrical symmetry in the angular distribution of the emitted secondary particles. Indeed, Fig. 2 shows that the raw time-of-flight spectra associated with the detectors belonging to the same row are nicely superimposed on top of each other without intensity correction. The overlap is further improved using a scaling factor per detector, which are interpreted as the *relative* detection efficiencies of these detectors. For all but one detector, the relative detection efficiency does not exceed 10% deviation from
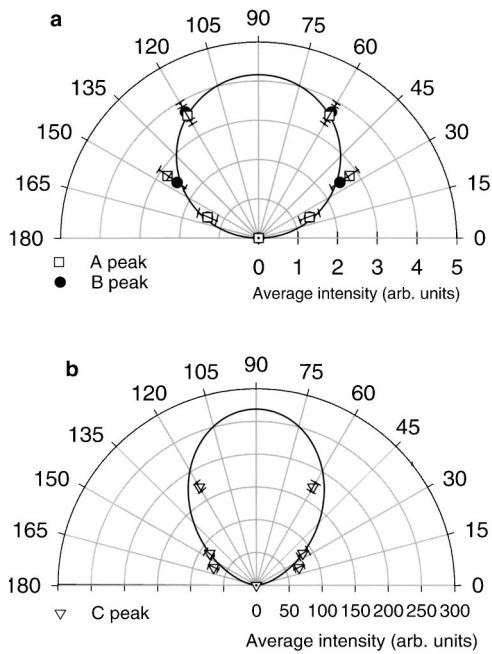
FIG. 3. Angular distributions corresponding to the three structures in the electron spectra. (a) A (open square) and B (full circle) peaks. (b) C peak (open triangle). Cosine (A and B peaks) and cosine-squared (C peak) distributions are drawn to guide the eyes.

the mean value associated with its row. Note that such a reasonable uniformity is observed only for the electron count rates in coincidence with the α particles where the detector background noise is completely washed out. The small count rate dispersion justifies *a posteriori* the tuning procedure of individual MCP detectors. This straightforward calibration among detectors of the same row already allows the multidetector to be used for study of azimuthal dependences. This relative calibration is the only definite result of this experiment, however, the very limited dispersion observed for the three different rows is very encouraging and suggests that variation of the average detection efficiency from one row to the other is probably less than a few percent. To compare detectors from different rows, we have assumed that in each row the detector with the highest detection efficiency has reached the absolute value of 80% often quoted when using a retention field.[7,8] An *absolute* detection efficiency ϵ_i can then be associated with each detector, allowing an evaluation of the doubly differential emission cross section. For a detector i specified by its polar angles θ_i, φ_i, the partial cross section is simply given by $\partial\sigma/\partial\Omega(\theta_i,\varphi_i)=I_i/(\Omega_d N_{ev}\epsilon_i)$ where I_i is the intensity integrated over the surface of the detector, Ω_d is the solid angle covered by the detector, ϵ_i the associated detection efficiency, and N_{ev} is the total number of trigger events. From the electron time of flight, the triply differential cross section $\partial\sigma/\partial E\partial\Omega(\theta_i,\varphi_i,E_i)$ with respect to the electron energy E_i can be derived. Since the azimuthal variation has been used for calibration, we focus here only on the polar angle dependence $\partial\sigma_p/\partial\Omega(\theta_i)$ associated with the three structures $p=A,B,C$ observed in the electron TOF spectra (Fig. 2). These are obtained as the relative weight of the three peaks in each TOF spectra times the averaged intensities measured in each row (Fig. 3). The intensity distri-

butions of the sharp peaks are found to follow a cosine distribution, whereas the intensity of the low-energy peak presents a narrower distribution closer to a $\cos^2$ distribution. From these rough angular distributions or from a fitted analytical form, the total cross section can be integrated. The result is expressed as the absolute emission yield associated with a given process per impact of an α particle. For the three peaks A, B, and C, the absolute yields amount to 0.3, 0.3, and 8 electrons, respectively. Combining the efficiency dispersion among the 15 detectors, with an estimated 10% uncertainty on the 80% detection efficiency assumed for the best detector in each row, an overall uncertainty of 15% can be attributed to the absolute yields. The observed distributions do not reflect the angular distribution in the bulk since transport in the solid and refraction at the surface affect the electron trajectories.[9–11] For electrons created in the bulk, a $\cos\theta$ angular dependence is commonly encountered resulting from the path length needed to reach the surface.[8,12] The observed cosine distribution for electrons associated with peaks A and B seems to corroborate the interrow calibration. For electrons with a kinetic energy which compares with the value of the work function, refraction on the surface potential further affects the electron trajectories by favoring more normal outgoing angles as actually observed here for low-energy electrons.

IV. ELECTRON ENERGY SPECTRA

Transformation of TOF spectra to energy spectra is particularly sensitive to the determination of the time origin t_o. In the present experiment, it takes 1.2 ns for a 5 MeV α particle to reach the pole detector and to deliver the ''start'' signal. This is confirmed by the weak peak (arrow in Fig. 2) on the right-hand side of the spectra which is interpreted as due to photons emitted during the foil crossing. The time-to-energy calibration is readily obtained knowing the 60 mm distance between the foil and the hemispherical grid just in front of the detectors. Figure 4 shows the average TOP row spectrum plotted in an energy scale, with [Fig. 4(a)] or without [Fig. 4(b)] the $E^{3/2}$ Jacobian weighting factor introduced in the time-to-energy transformation. Figure 4(b) ressembles the TOF spectrum and is presented only to highlight the high-energy side, whereas Fig. 4(a) should directly compare with spectra recorded with the electrostatic analyzer.[9,13–16] The two ''sharp'' structures now appear at 66 ± 12 eV (60 eV width) and 10.5 ± 1.1 eV (3.3 eV width), respectively, while the continuous spectrum peaks around 3.00 eV with a 2.25 eV width. The high-energy peak can be unambiguously attributed to the aluminum LVV Auger electrons, well known in electron and ion interactions with aluminum targets.[17–19] The 10.5 eV peak is ascribed to the decay of volume *plasmons* [$\hbar\omega=15.3$ eV (Refs. 13–16)], whose energy is transferred to a single electron which has to overcome the assumed $\Phi_0=4.3$ eV work function ($E_c\leqslant\hbar\omega-\Phi_0$). Our 3.3 eV experimental width has to be compared with the 2 eV natural width given by the plasmon lifetime[16] and an experimental resolution of 1 eV at this energy.

Volume plasmons have already been observed in electron spectroscopy by numerous authors,[9,12–14] such as Drex-
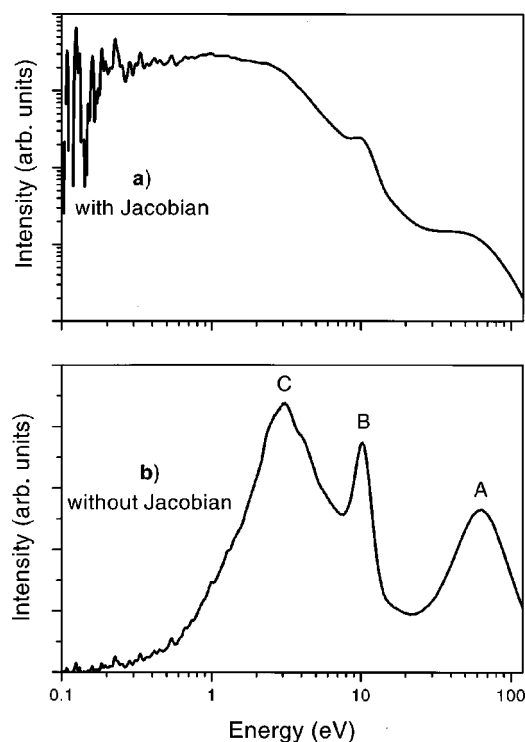
FIG. 4. TOF spectra recorded on the TOP row are averaged and plotted on an energy scale. In plot (b) the counts recorded at a time t are simply plotted at the corresponding energy $E \propto 1/t^2$, whereas in plot (a) the counts are normalized with proper account of the Jacobian to produce the correct intensity ratio. The two spectra show three structures, A, B, and C, identified in the TOF spectra corresponding, respectively, to LVV Auger (66 eV), volume plasmons (10.5 eV), and low-energy electrons (3 eV).

ler and DuBois[9] for MeV protons traversing a thin carbon foil or Hasselkamp and Scharmann[14] for 500 keV H$^+$, He$^+$, and Ar$^+$ ions on clean or oxidized aluminum targets. In these investigations the plasmon peak hardly appears as a change of slope on the high-energy side of the 3 eV background electrons. The most striking feature of the present spectra is the comparatively good contrast of the volume plasmon peak despite the oxide layer of 40 Å maximum thickness[20] covering our target. The expected enhancement of the contribution of the low-energy electrons from this overlayer[14] does not seem to spoil the resolution of the volume plasmon peak. The observed contrast between volume plasmons and low-energy background electrons may be reasonably attributed to the use of a high-velocity doubly charged projectile[16] or to the forward detection geometry.

V. DISCUSSION

We have successfully calibrated a set of MCP detectors using a very compact and comparatively safe sealed radioactive alpha source of low activity. The impact of the 5 MeV alpha particles through a thin aluminum foil produces typical secondary electron energy spectra. The uncontrolled oxide layer covering the foil does not smear out the characteristic

energy spectrum consisting of three well-identified structures around 3, 10, and 66 eV. The two higher-energy peaks have been ascribed, respectively, to the aluminum Auger electrons and to the decay of aluminum plasmons. Comparison with the characteristic peak energies derived following the time-to-energy transformation provides a useful confirmation of our energy-scale calibration. Exploiting the specific symmetry of the emission processes, the relative detection efficiency for three groups of MCP based detectors is achieved. From the observed intrarow uniformity, the calibration is extended to different rows and seems to be validated by the observed angular distribution. Although determination of the absolute efficiency relies on a normalization parameter, this type of experiment gives very reproducible results and provides a simple and reliable means to check the relative detection efficiency of a complex device.

[1] V. A. Morosov, A. Kalinin, Z. Szilagyi, M. Barat, and P. Roncin, Rev. Sci. Instrum. **67**, 2163 (1996).
[2] C. Lemell, J. Stockl, H. P. Winter, and F. Aumayr, Rev. Sci. Instrum. **70**, 1653 (1999).
[3] J. L. Wisa, Nucl. Instrum. Methods **162**, 587 (1979).
[4] E. Browne and R. B. Firestone, *Table of Radioactive Isotopes* (Wiley, New York, 1986).
[5] J. F. Ziegler, J. P. Biersack, and U. Littmark, *The Stopping and Range of Ions in Solids* (Pergamon, New York, 1985).
[6] G. Pashmann, E. G. Shelley, C. R. Chappell, R. D. Sharp, and L. F. Smith, Rev. Sci. Instrum. **41**, 1706 (1970).
[7] R. Cordia Taylor, M. C. Hettrick, and R. F. Malina, Rev. Sci. Instrum. **54**, 171 (1983).
[8] B. L. Doyle, G. Vizkelethy, D. S. Walsh, B. Senftinger, and M. Mellon, Nucl. Instrum. Methods Phys. Res. B **158**, 6 (1999).
[9] C. G. Drexler and R. D. DuBois, Phys. Rev. A **53**, 1630 (1996).
[10] S. Hufner, Springer Ser. Solid-State Sci. **82**, 246 (1995).
[11] P. Sigmund and S. Tougaard, Springer Ser. Chem. Phys. **17**, 2 (1981).
[12] A. Jablonski, I. S. Tilinin, and C. J. Powell, Phys. Rev. B **54**, 10927 (1996).
[13] J. Pillon, D. Roptin, and M. Cailler, Surf. Sci. **59**, 741 (1976).
[14] D. Hasselkamp and A. Scharmann, Surf. Sci. **119**, L388 (1982); D. Hasselkamp, Comments At. Mol. Phys. **21**, 241 (1988).
[15] R. Baragiola and C. Dukes, Phys. Rev. Lett. **76**, 2547 (1996).
[16] S. M. Rizau, R. Baragiola, and R. C. Monreal, Phys. Rev. B **59**, 15506 (1999).
[17] M. Herteux, W. Hink, J. P. Biersack, and E. Scherck, Nucl. Instrum. Methods Phys. Res. B **48**, 621 (1990).
[18] A. Koyama, O. Benka, H. Ishikawa, T. Iitaka, Y. Sasa, and M. Uda, Nucl. Instrum. Methods Phys. Res. B **75**, 86 (1993).
[19] A. Bonanno, N. Mandarino, A. Oliva, and F. Xu, Nucl. Instrum. Methods Phys. Res. B **71**, 161 (1992).
[20] C. C. Chang, T. A. Callcott, and E. T. Arakawa, Phys. Rev. B **32**, 6138 (1985).